

RESEARCH

Open Access



Neuropathological contributions to grey matter atrophy and white matter hyperintensities in amnesic dementia

Diana Ortega-Cruz^{1,2}, Alberto Rabano² and Bryan A. Strange^{1,2*}

Abstract

Background Dementia patients commonly present multiple neuropathologies, worsening cognitive function, yet structural neuroimaging signatures of dementia have not been positioned in the context of combined pathology. In this study, we implemented an MRI voxel-based approach to explore combined and independent effects of dementia pathologies on grey and white matter structural changes.

Methods In 91 amnesic dementia patients with post-mortem brain donation, grey matter density and white matter hyperintensity (WMH) burdens were obtained from pre-mortem MRI and analyzed in relation to Alzheimer's, vascular, Lewy body, TDP-43, and hippocampal sclerosis (HS) pathologies. After exploring co-occurrence profiles of these pathologies, voxel-based morphometry was implemented to determine their joint and independent effects on grey matter loss. The impact of these pathologies on WMH burden was then evaluated both in spatial and quantitative combined analyses, using voxel-based and generalized linear models respectively.

Results 86.8% of patients in this cohort presented more than one pathology. The combined structural effect of these pathologies was a focal impact on hippocampal grey matter atrophy, primarily driven by HS and Alzheimer's pathology (family-wise error corrected, $p < 0.05$), which also exhibited the strongest individual effects (uncorrected, $p < 0.001$). WMHs, predominant in middle and anterior cerebral portions, were most strongly associated with vascular ($T = 2.47$, $p = 0.017$) and tau pathologies ($T = 2.09$, $p = 0.041$).

Conclusions The mixed associations of these dementia neuroimaging hallmarks are relevant for the fine-tuning of diagnostic protocols and underscore the need for comprehensive pathology evaluations in the study of dementia phenotypes.

Keywords Combined pathology, Grey matter atrophy, Magnetic resonance imaging, Neuroimaging, Structural biomarkers, White matter hyperintensities, Whole-brain

*Correspondence:

Bryan A. Strange
bryan.strange@upm.es

¹Laboratory for Clinical Neuroscience, Center for Biomedical Technology, Universidad Politécnica de Madrid, IdiSSC, Crta M40, km38, Madrid 28223, Spain

²Alzheimer's Disease Research Unit, CIEN Foundation, Queen Sofia Foundation Alzheimer Center, Madrid 28031, Spain



© The Author(s) 2024. **Open Access** This article is licensed under a Creative Commons Attribution-NonCommercial-NoDerivatives 4.0 International License, which permits any non-commercial use, sharing, distribution and reproduction in any medium or format, as long as you give appropriate credit to the original author(s) and the source, provide a link to the Creative Commons licence, and indicate if you modified the licensed material. You do not have permission under this licence to share adapted material derived from this article or parts of it. The images or other third party material in this article are included in the article's Creative Commons licence, unless indicated otherwise in a credit line to the material. If material is not included in the article's Creative Commons licence and your intended use is not permitted by statutory regulation or exceeds the permitted use, you will need to obtain permission directly from the copyright holder. To view a copy of this licence, visit <http://creativecommons.org/licenses/by-nc-nd/4.0/>.

Background

Compared to other imaging techniques, magnetic resonance imaging (MRI) is a minimally invasive and cost-effective method providing a comprehensive perspective in the identification of dementia [1]. Atrophy patterns on structural MRI have been characterized for each type of dementia and are today included within specific diagnostic criteria for Alzheimer's Disease (AD), vascular dementia (VaD), Dementia with Lewy Bodies (DLB) and Frontotemporal Dementia (FTD) [2, 3]. These patterns have also been employed to differentiate each type, with one study reaching 70.6% classification accuracy using solely MRI-derived features [4]. Grey matter atrophy profiles are especially useful to identify AD (especially affecting the temporal lobe), FTD (with frontal and temporal lobes affected, variably across phenotypic subtypes) and DLB (occipital and subcortical atrophy). However, the impact of combined pathology, present in over half of late-onset dementia patients [5], affects the interpretability of grey matter (GM) atrophy profiles typically associated with different types of dementia. While several GM-focused MRI studies have considered the contribution of co-pathologies [6–11], they have focused on specific regions of interest, such as the basal forebrain, hippocampus or brain ventricles. The inconsistency between considered regions and pathologies limits the joint interpretation of the findings from previous work into clinically relevant structural patterns.

In contrast to these grey matter signatures, the detection of VaD relies on finding specific lesions such as infarcts, lacunes or white matter hyperintensities (WMHs) [12–14]. Most evident on fluid-attenuated inversion recovery (FLAIR) MRI, WMHs are a general hallmark of aging, while also associated with cognitive worsening [15] and a three-fold higher risk of dementia [16]. The prevalence of WMHs is higher in individuals with vascular risk factors such as hypertension and diabetes [17], as well as in those with more specific cerebrovascular conditions [18]. As a result, WMHs are widely used as a VaD biomarker, commonly assessed through visual rating systems such as Fazekas [19] and Scheltens [20] scales. However, these lesions are not specific to vascular pathology, as higher WMH burden has also been found in AD [21], independently of comorbid vascular disease [22]. Further studies found an association between WMHs and amyloid- β (A β), but not tau pathology [23–25], although others reported the opposite [26, 27]. This discrepancy might be driven by differences in WMHs assessment as well as in the technique employed for measuring A β and tau burdens, ranging from *in vivo* CSF or PET biomarkers to postmortem histopathology evaluation.

Another factor limiting the understanding of WMH pathologic correlates, and their specificity, is again the

lack of consideration of coexistence of dementia neuropathologies [28], which is known to lead to more severe cognitive syndromes [29]. For example, previous studies evaluated the contribution of tau and A β on WMHs separately [27], or disregarded the contribution of other co-pathologies [24, 26], or both [23]. Up to now, only one study evaluated WMH burden as a function of a comprehensive array of pathologies within the same analytical model [25], reporting an association with vascular (arteriosclerosis and gross infarcts) and A β pathologies.

In the current study, we explored the combined effect of dementia neuropathologies on brain atrophy and WMH burden during advanced disease stages. We leveraged pre-mortem MRI and post-mortem pathology data from the Vallecas Alzheimer's Center Study, a cohort of institutionalized dementia patients with a primarily amnesic profile. Considering AD, vascular, Lewy body, TDP-43 pathologies and hippocampal sclerosis of aging, we performed MRI-pathology correlational analyses in a group of 91 patients. The specific aims of this study were threefold: (i) to evaluate the separate and combined contribution of these pathologies on whole-brain atrophy differences; (ii) to assess their impact on WMH burden, while verifying its debated association with tau or A β ; and (iii) to study the spatial distribution of WMHs across cerebral vascular territories and in relation to this set of pathologies. Our study illustrates quantitative and whole-brain structural signatures of dementia neuropathologies that can optimize the clinical use of MRI as a biomarker.

Methods

Cohort and MRI features

The Vallecas Alzheimer's Center Study (VACS) is a follow-up program for dementia patients in a specialized nursing home. The program includes clinical and MRI evaluations, as well as the possibility of post-mortem brain donation to the BT-CIEN brain bank ('Banco de Tejidos Fundación CIEN', in Spanish). For this study, we analyzed data from patients with at least one usable pre-mortem MRI scan (as specified below) and post-mortem brain donation. Cognitive performance was considered based on the severe Mini-Mental State Examination (sMMSE), a version of the standard MMSE test adapted for individuals with severe cognitive impairment [30]. Test scores from baseline (at admission) and pre-exitus (penultimate prior to death) follow-up visits were retrieved.

Magnetic resonance images were acquired using a 3T scanner (Signa HDxt General Electric), using a phased array 8 channel head coil. For T1-weighted images, 3D sagittal fast spoiled gradient recalled (FSPGR) configuration was used with inversion recovery (repetition/echo/inversion time 7/3.2/750ms, slice thickness 1 mm, matrix 288×288, field of view 240 mm, final resolution

1 × 0.469 × 0.469 mm). For subjects experiencing difficulties staying still in the scanner, an alternative protocol for faster T1-weighted imaging was used (slice thickness 2 mm, matrix 200 × 200, field of view 220 mm, final resolution 1 × 0.859 × 0.859 mm). FLAIR images were acquired using 2D axial fast spin echo (FSE) configuration with inversion recovery (9000/124/2500ms, slice thickness 3.4 mm, no interslice gap, resolution 0.938 × 0.938 × 3.4 mm). The quality of acquired scans was evaluated by an experienced neuroradiologist, who also performed Fazekas scoring on FLAIR images (evaluation of periventricular and deep WMHs, each on a score 0–3 [19]). Scans with no motion artifacts hindering distinction of tissue boundaries (white, grey matter and CSF) and thereby reliable segmentation, were selected. To correlate MRI measurements to pathological data, we retrieved the last T1-weighted (available for 97 patients) and FLAIR (88 patients) images of sufficient quality. For selected FLAIR images from each patient, the T1-weighted scan from the same session was obtained as well.

Neuropathological evaluation

Post-mortem brain extraction was performed according to the BT-CIEN protocol [31] by an experienced neuropathologist. The left hemisphere was fixed, coronally sliced and used to obtain histological sections from relevant regions for neuropathological evaluation. Sections were stained with hematoxylin/eosin (H/E) as well as immunostained with primary antibodies against A β , phosphorylated tau (AT100), total α -synuclein and total TDP-43.

Established consensus criteria were used to evaluate the following neuropathological burdens: Alzheimer's Disease Neuropathological Change (ADNC, 0–3) [32] (based on assessment of Thal stage for A β , Braak tau stage and neuritic plaque density), Braak α -synuclein stage [33] (0–6) for Lewy body (LB) pathology distribution, and limbic-predominant age-related TDP-43 encephalopathy (LATE) staging [34] (0–3). Cerebrovascular pathology was evaluated following two proposed consensus evaluations: Deramecourt scoring (0–20) [35] and Vascular Cognitive Impairment Neuropathology Guidelines (VCING, 1–3) [36]. The former evaluates vascular pathology events in various regions using a hierarchical scoring based on their incidence, while the latter is a composite score including evaluation of cerebral amyloid angiopathy (CAA), arteriolosclerosis, and large infarcts. Finally, hippocampal sclerosis of aging (HS) was evaluated in the hippocampal head following our recently proposed H/E-based staging system (0-IV) [37] including early gliotic stages.

To assess the coexistence between pathologies, the following thresholds were used to determine a high burden

of each of them: high ADNC (score of 3), LB pathology in limbic or neocortical regions (3 or higher), TDP-43 hippocampal pathology (2 or higher), Deramecourt score 8 or higher, and early or advanced HS (stages I to IV).

Grey and white matter segmentation

T1-weighted images were processed for voxel-based morphometry (VBM) using SPM12 software (version v7771). First, images were modulated, homogenized in intensity, resliced to 2 mm and segmented into grey matter, white matter, and cerebrospinal fluid. The Diffeomorphic Atlas Registration Tool with Exponentiated Lie Algebras (DARTEL) technique was then used to spatially register segmentations to an in-house template, constructed from 348 scans of elderly subjects from previous studies at the Vallecas Alzheimer Center. Finally, registered maps were normalized to the Montreal Neurological Institute (MNI) atlas by affine transformation and smoothed with a Gaussian kernel of 6 mm. To discard relevant anatomical or segmentation differences, images were assessed using the sample homogeneity tool from the Computational Anatomy Toolbox (CAT12) [38]. At this step and together with visual inspection, 10 out of 97 subjects were determined to present inaccurate grey-white matter boundary segmentations. Out of these, we attempted to correct 7 segmentations which were affected by high WMH burdens. For that purpose, we used the Lesion Segmentation Toolbox (LST, version 3.0.0) within SPM12. WMHs were first segmented from T1 and FLAIR images from the same time point using the Lesion Prediction Algorithm from LST, followed by lesion filling in the T1 image [39]. After reapplying all VBM processing steps to the 7 filled images, 4 were finally included as visually acceptable grey-white matter segmentations. Therefore, data from 6 subjects was excluded and a total of 91 subjects were included in these analyses. Out of these included T1 images, 31.9% were acquired using the faster scanning protocol described above.

WMH segmentation

We measured WMH burden using automated segmentation methods, which offer greater reproducibility and eschew ceiling effects associated with visual scales. To evaluate the most suitable method for our dataset, we obtained WMH segmentations for all subjects using four approaches: two LST algorithms [39], (a) Lesion Prediction Algorithm (LPA) and (b) Lesion Growth Algorithm (LGA); (c) Samseg WMH segmentation [40]; and (d) FreeSurfer 7.1.1 subcortical segmentation. Variable inputs were used for each method: only FLAIR for (a), FLAIR and T1 sequences for (b) and (c), and only the T1 image for method (d). A default initial threshold of 0.3 was used for LGA, which was afterwards validated as the

optimal value. As hyperintense artifacts can be found in ventricles in FLAIR images, subcortical segmentations from FreeSurfer were aligned to FLAIR images to remove ventricle areas from LPA WMH maps. Resulting segmentations were visually inspected, and out of 88 subjects in this dataset, 5 were discarded due to strong over- or underestimation of WMHs in at least two of the four methods. WMH volumes from the included 83 subjects were then obtained from each segmentation, using an intensity threshold of 0.5 for LST lesion maps.

Voxel-based morphometry

Obtained grey, white matter and WMH segmentations were analyzed at the group level using general linear models in SPM12. Explanatory variables included in each model were sex, age at scan, MRI antemortem interval (AMI), T1 acquisition protocol, total intracranial volume (TIV), and neuropathological stages of interest. For grey and white matter maps derived from T1-weighted images, the following neuropathological stages were included: ADNC, Deramecourt vascular score, Braak α -synuclein stage, LATE and HS staging. Individual T-contrasts were used to evaluate an inverse relation of each variable with tissue density, and a combined F-contrast was used to determine whether significant variance is explained by the neuropathological variables (i.e., to probe for independent and combined, positive or negative effects across all pathologies). For WMH maps, pathological explanatory variables included were Thal A β stage, Braak tau stage, Deramecourt score, Braak α -synuclein stage, LATE and HS staging.

In addition to these pathology models, differences in grey matter density were analyzed as a function of cognitive state. For that, regions with a significant correlation to pre-exitus sMMSE scores were evaluated, correcting for sex, age at scan, acquisition protocol, TIV, and time between MRI and cognitive evaluation. All results were reported at $p < 0.05$ using family-wise error (FWE) correction for multiple comparisons, with uncorrected results reported descriptively at a threshold of $p < 0.001$. Using CAT12, Threshold-free cluster enhancement [41] (1000 permutations) was applied to WMH maps prior to FWE correction, restricting results with a WM mask to avoid partial volume effects at the boundary with GM. This method enhances the sensitivity to spatially extended results by accounting for the added contribution of neighboring voxels. The Automated Anatomical Labelling Atlas 3 (AAL3) [42] was used to assign neuro-anatomical regions to result maps.

Statistical analyses

Apart from VBM, all analyses and plots were performed using RStudio 1.4.1106. Pearson's correlations were used to compare results from WMH segmentation methods

with visual Fazekas scores. To examine the dependence of WMH volume on combined pathology, we employed a generalized linear model (GLM), which accommodates non-normal distributions while preserving the natural range of studied values. The GLM included the same neuropathological stages and covariates as the WMH VBM model. Similarly to SPM12 analyses, neuropathological stages (ordinal evaluations) were treated as numeric to enable the modelling of subtle variations in quantitative MRI measures. A summary of the voxel-wise and volume models developed in this study to explore combined pathology effects is provided in Supplementary Table 1.

To explore the relationship between WMH volumes and individual vascular pathologies, GLMs were applied including three sub-scores derived either from Deramecourt or VCING evaluations (as well as TIV, sex, age and AMI as covariates). To spatially compare WMH burdens, lesion segmentations were masked using a vascular territory atlas [43] and resulting volumes were normalized by WM volume in each territory. Regional WMH volumes were then compared across territories (anterior, middle, posterior) and hemispheres (left/right) using repeated measures ANOVA with post-hoc pairwise T tests. Finally, cognitive state was also analyzed as a function of WMHs using baseline and pre-exitus sMMSE scores. These were regressed as a function of WMH volume, TIV, sex, age at scan, and time between MRI and cognitive evaluation.

All RStudio models were run in the absence and presence of dependent-variable outliers (deviating more than 1.5 times the interquartile range), and the most conservative results were chosen. A p value below 0.05 was considered statistically significant.

Results

Neuropathological profiles

The VACS cohort is composed of a predominantly female population, with advanced age at symptom onset and long disease duration. Out of the 91 subjects included in our T1-derived analyses, 83.5% were females and the average age at death was 87.9 ± 6.7 years. Additional demographic and pathology details of this population are provided in Supplementary Table 2. As expected, there was a high incidence of co-pathologies in this group (Fig. 1A), with 86.8% of patients presenting more than one pathology. Only 10 subjects presented a high burden of a single pathology (two subjects presented only high ADNC, and eight presented only high vascular burden), which could be classified as "pure" AD and vascular cases, respectively. Interestingly, 14 subjects presented concomitant high burdens of the five studied pathologies. Two subjects presented only low pathology burdens, and thus were not included in Fig. 1A. The correlation between these neuropathological stages was also explored to aid the interpretation of subsequent analyses.

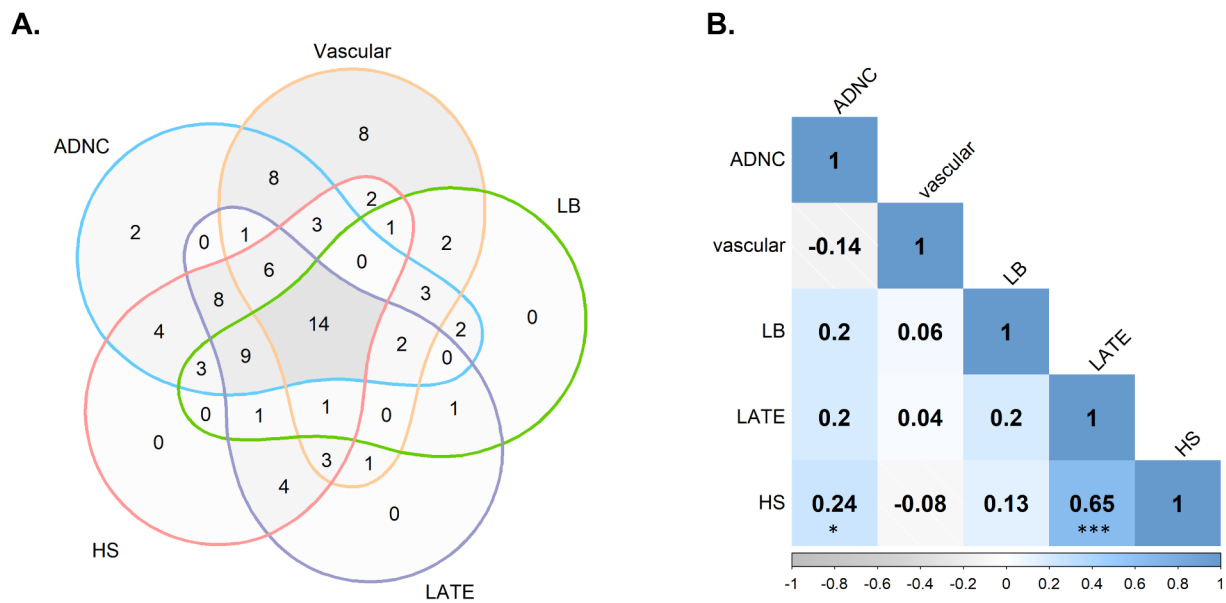


Fig. 1 Associations between pathological burdens in the studied cohort. **(A)** Venn diagram showing the co-occurrence of high burdens for each neuropathology. High-burden thresholds are defined as specified in the Methods (Neuropathological Evaluation section). **(B)** Correlation matrix between included pathological stages, showing Spearman's correlation coefficients and significance indicators: $p < 0.05$ (*) and $p < 0.001$ (***). ADNC = Alzheimer's Disease Neuropathological Change; HS = hippocampal sclerosis of aging; LATE = Limbic Predominant Age-Related TDP-43 Encephalopathy; LB = Lewy body pathology

As shown in Fig. 1B, HS and LATE stages were the two most highly correlated pathologies, followed by HS and ADNC.

Combined and independent pathological contributions to atrophy

Given the heterogeneous neuropathological profiles present in this cohort, we evaluated the effect of global pathology severity on structural brain differences at the time point closest to death. T1-weighted images, with an average antemortem interval (AMI) of 3.04 ± 3 years, were used to derive grey and white matter tissue maps. Grey matter density (GMD) was then compared voxel-wise between subjects, considering the five evaluated pathologies using an F-test (summary of model details in Supplementary Table 1). As can be seen in Fig. 2A, global pathology severity was associated with focal bilateral grey matter loss in the medial temporal lobe. These effects, surviving whole-brain FWE correction, extended from the amygdala to the hippocampal tail in both hemispheres, including the left parahippocampal gyrus as well. We also averaged contrast estimates (model coefficients of the contribution of each variable to the results) within the region displaying significant effects. Figure 2B shows grey matter loss in this region was driven primarily by HS severity and ADNC, with a minor contribution of vascular, LB and TDP-43 pathologies.

Using the same statistical model, single-variable contrasts were used to explore GMD differences as a

function of each individual pathology. Therefore, individual pathology effects were analyzed while accounting for other co-pathologies as covariates. As shown in Fig. 3A, after applying FWE correction for multiple comparisons, HS stage was the only pathological variable presenting a significant negative correlation with GMD. These effects were restricted to bilateral temporal regions, more specifically to the parahippocampal gyri. At an uncorrected level, voxel-wise GMD differences associated with each pathological variable are shown in Fig. 3B. ADNC was associated with significant uncorrected effects in the right middle temporal gyrus, amygdala, hippocampus, and left fusiform gyrus. LB pathology showed effects in the right orbital and fusiform gyri and left superior temporal and lingual gyri. Minimal GMD differences were observed as a function of vascular and TDP-43 pathologies. MNI coordinates and labels for all corrected and uncorrected results are specified in Supplementary Table 3.

Interestingly, more prominent effects of TDP-43 were observed bilaterally in the hippocampus when HS was removed from the model, such that the strong correlation between LATE and HS stages renders these effects non-significant in the original model (Supplementary Fig. 1, Additional File 1). We also examined voxel-wise differences in white matter density, with no combined nor individual pathology effects displaying significance at $p < 0.05$ after FWE correction. Additionally, the relation between cognitive worsening and grey matter loss

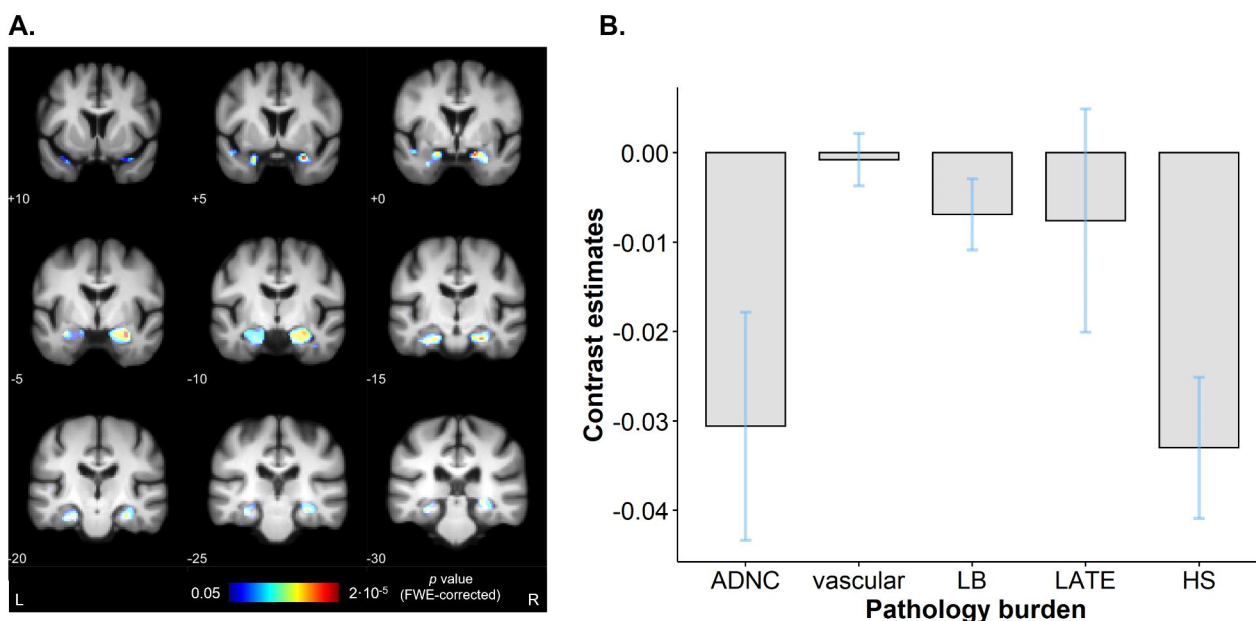


Fig. 2 Combined contribution of the studied neuropathologies to grey matter loss. **(A)** Voxel-based morphometry results as a function of all neuropathologies, surviving whole-brain FWE correction for multiple comparisons. Results are thresholded at $p < 0.05$ and overlaid on an in-house template built from scans of elderly subjects. MNI coronal coordinates are provided, as well as left and right-side labels. Colormap indicates FWE-corrected p values. **(B)** Contrast estimates (effect sizes) for each variable, showing their effect on grey matter density in the region displaying significant effects (predicted density = $\sum(\text{Contrast estimate}) \cdot (\text{Pathology stage})$ through the five pathologies). Blue bars indicate 90% confidence interval. ADNC = Alzheimer's Disease Neuropathological Change; FWE = family-wise error; HS = hippocampal sclerosis of aging; L = left; LATE = Limbic Predominant Age-Related TDP-43 Encephalopathy; LB = Lewy body pathology; MNI = Montreal Neurological Institute; R = right

was studied in a separate model using pre-exitus sMMSE scores. This analysis revealed significant results in temporal and subcortical regions, with strongest effects in the right insula and left caudate nucleus (Supplementary Fig. 2).

Impact of neuropathologies on WMH volume

Next, we implemented a similar approach to evaluate the contribution of combined pathology to WMH burden. First, we determined the most optimal WMH quantification method for this dataset among four freely available methods that did not require prior training: Lesion Prediction (LPA) and Lesion Growth (LGA) algorithms from the LST toolbox, Samseg, and FreeSurfer standard subcortical segmentation. Examples from segmentation outcome at different levels of WMH burden can be observed in Supplementary Fig. 3. WMH volumes obtained from these automated methods were compared relative to Fazekas scores, which are widely used in the clinical context. As shown in Supplementary Fig. 4, all volume measures significantly correlated with Fazekas scores for periventricular and deep WMH, with correlation coefficients being highest for LPA. Therefore, LPA WMH volumes were used in subsequent analyses as the most clinically relevant measure among the four tested methods. Out of the 83 subjects with successful WMH processing, 79 were included in subsequent analyses

after visual quality control of LPA segmentations. The suitability of this WMH measure was further validated by exploring its association with cognition, based on sMMSE scores. Correcting for demographic differences, both baseline and pre-exitus sMMSE scores were significantly lower with increasing WMH burdens (Supplementary Fig. 5), in line with the expected effect of these lesions on symptom severity.

To assess the relation between mixed pathology and LPA-derived WMH volumes, a generalized linear model was used including AD, vascular, LB, LATE and HS pathologies, while correcting for demographic differences (as summarized in Supplementary Table 1). Here, AD pathology was separately modelled using tau and A β pathology stages to address discrepancies between previous studies regarding their effects on WMHs. As shown in Fig. 4, this combined model showed tau and vascular pathologies were associated with greater WMH volume, while its associations with HS stage reached trend-level significance. As an antemortem interval longer than 3 years has been shown to increase the chances of underestimating MRI-derived WMH burden relative to post-mortem quantification [25], we repeated this analysis only including patients with an AMI below 3 years ($n = 49$). In this subset of the cohort, vascular pathology and HS displayed a significant effect on WMH burden (Supplementary Fig. 6).

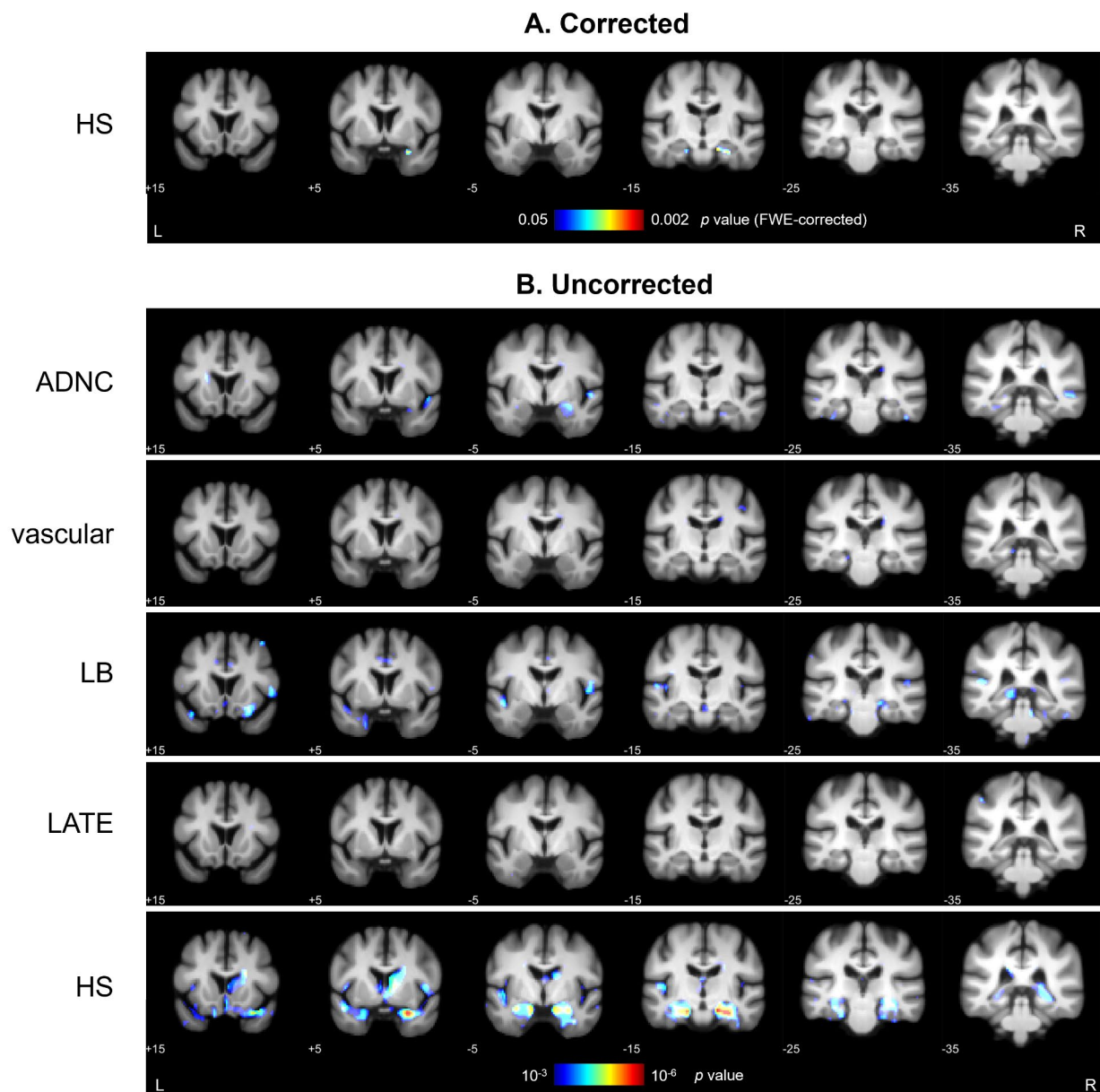


Fig. 3 Individual pathology effects on grey matter density differences. **(A)** Results after applying whole-brain FWE correction for multiple comparisons, with significant effects ($p < 0.05$) surviving only as a function of HS stage. **(B)** GMD correlates of all studied pathologies of the general linear model, thresholded at $p < 0.001$ uncorrected. MNI coordinates are provided below each coronal section, and colormap indicates p values within the specified ranges. Specific coordinates and labels for these results are provided in Supplementary Table 3. ADNC = Alzheimer's Disease Neuropathological Change; FWE = family-wise error; HS = hippocampal sclerosis of aging; L = left; LATE = Limbic Predominant Age-Related TDP-43 Encephalopathy; LB = Lewy body pathology; MNI = Montreal Neurological Institute; R = right

We also evaluated the contribution of the VCING assessment of vascular pathology, as an alternative to Deramecourt score. Although subjects with a high VCING score presented greater WMH volumes (Supplementary Fig. 7), no significant associations were found in the combined model, regardless of whether we included all patients or the shorter-AMI patient subset. Additionally, differences between vascular assessments were

further explored by regressing WMH volumes as a function of Deramecourt or VCING sub-scores separately (Supplementary Fig. 8). These analyses identified a significant relation between WMH burden and vessel wall alterations (CAA or arteriolosclerosis) derived from Deramecourt scores, while no significant effects were found for VCING sub-scores.

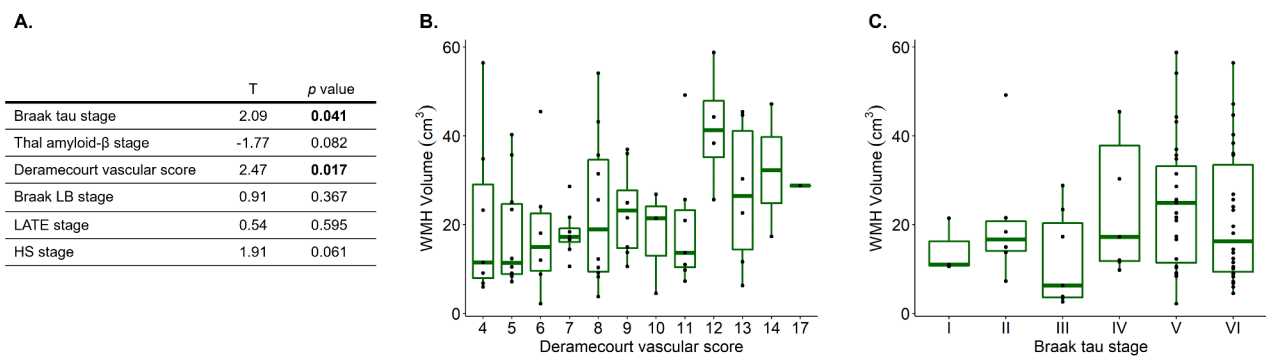


Fig. 4 Results from modelling LPA WMH volumes as a function of combined pathology. **(A)** Results from the generalized linear model including 6 pathological variables of interest. T-statistics and *p* values for each independent variable of interest are provided, with *p* values below the significance threshold (<0.05) highlighted in bold. **(B)** Boxplot showing the distribution of WMH volumes as a function of Deramecourt vascular score, which shows the strongest contribution in the combined model. **(C)** Boxplot of WMH volume as a function of Braak tau stage, with a significant effect in the combined model. HS = hippocampal sclerosis of aging; LATE = Limbic Predominant Age-Related TDP-43 Encephalopathy; LB = Lewy body pathology; LPA = Lesion Prediction Algorithm; WMH = white matter hyperintensity

Spatial WMH pathology signatures

To evaluate the spatial specificity of these quantitative results, we explored the anatomical distribution of WMHs in this cohort. LPA-derived WMH maps were first divided into 3 bilateral territories [43] according to cerebral vasculature: anterior, middle and posterior cerebral arteries. Normalized WMH volumes per territory were significantly higher in the middle compared to the anterior region ($F(2,460) = 22.7$, $p < 0.01$), being both significantly higher than posterior burden ($p < 0.001$ for both comparisons). No significant differences in WMH volume were found between hemispheres ($F(1,460) = 0.09$, $p = 0.76$).

Next, we used VBM to assess voxel-wise correlations of LPA WMH maps with combined pathology. This analysis included the same independent pathological staging variables as in the previous section. In line with our previous results, tau and vascular stages were the only variables with effects surviving correction for multiple comparisons. Surprisingly, WMH regions that significantly correlated with both tau and vascular burden were lateralized to the right hemisphere, as shown in Fig. 5. These results were also predominant in anterior and middle vascular territories, with strongest effects localizing within the right pre- and post-central gyri for Deramecourt score, and within the right precuneus and angular gyrus for Braak tau stage. No results as a function of all pathologies combined survived correction, while uncorrected results were predominant in the right precentral region as well.

Discussion

Using pre-mortem MRI from amnesic dementia patients, this study aimed to illustrate structural correlates of brain atrophy and WMHs in the context of combined pathology. We found that the combined impact of dementia neuropathologies is associated with a marked,

focal grey matter loss in the hippocampus. These effects were mainly driven by HS severity and Alzheimer's pathology burden. Exploring individual pathology effects on GM loss, we again found strongly reduced hippocampal GMD as a function of HS, with ADNC and LB also presenting significant effects at an uncorrected threshold. The right lateralization of individual ADNC effects in the medial temporal lobe may serve to decompose the contribution of this variable in the combined model, in which model coefficients were averaged across significant results from both hemispheres. Vascular pathology was not found to correlate with GM loss, in line with previous studies considering combined pathology [7, 11]. While no pathological effects were found on white matter density, we specifically explored pathological vulnerabilities of this tissue based on WMHs. These analyses showed vascular and tau pathologies are the strongest contributors to WMH burden, while also suggesting an independent effect of HS which remains currently unexplored.

Our findings therefore support the previously reported link between AD and WMHs independently of comorbid vascular pathology [21–23]. However, employing a similar combined approach to measuring WMH correlates, Arfanakis et al. reported a contribution of $A\beta$ rather than tau [25]. Although those findings were obtained with a larger sample size of 603 individuals, covering a wider cognitive range, they were based on Fazekas scoring rather than quantitative measurements. Besides, this previous study averaged $A\beta$ and tau burdens across regions instead of following diagnostic criteria, which might further contribute to the discrepancy with our results. One asset of our approach lies in addressing this research question from two different perspectives (volume- and voxel-based), such that the consistency between both results supports their reliability. Voxel-based analyses revealed vascular and tau pathology burdens specifically

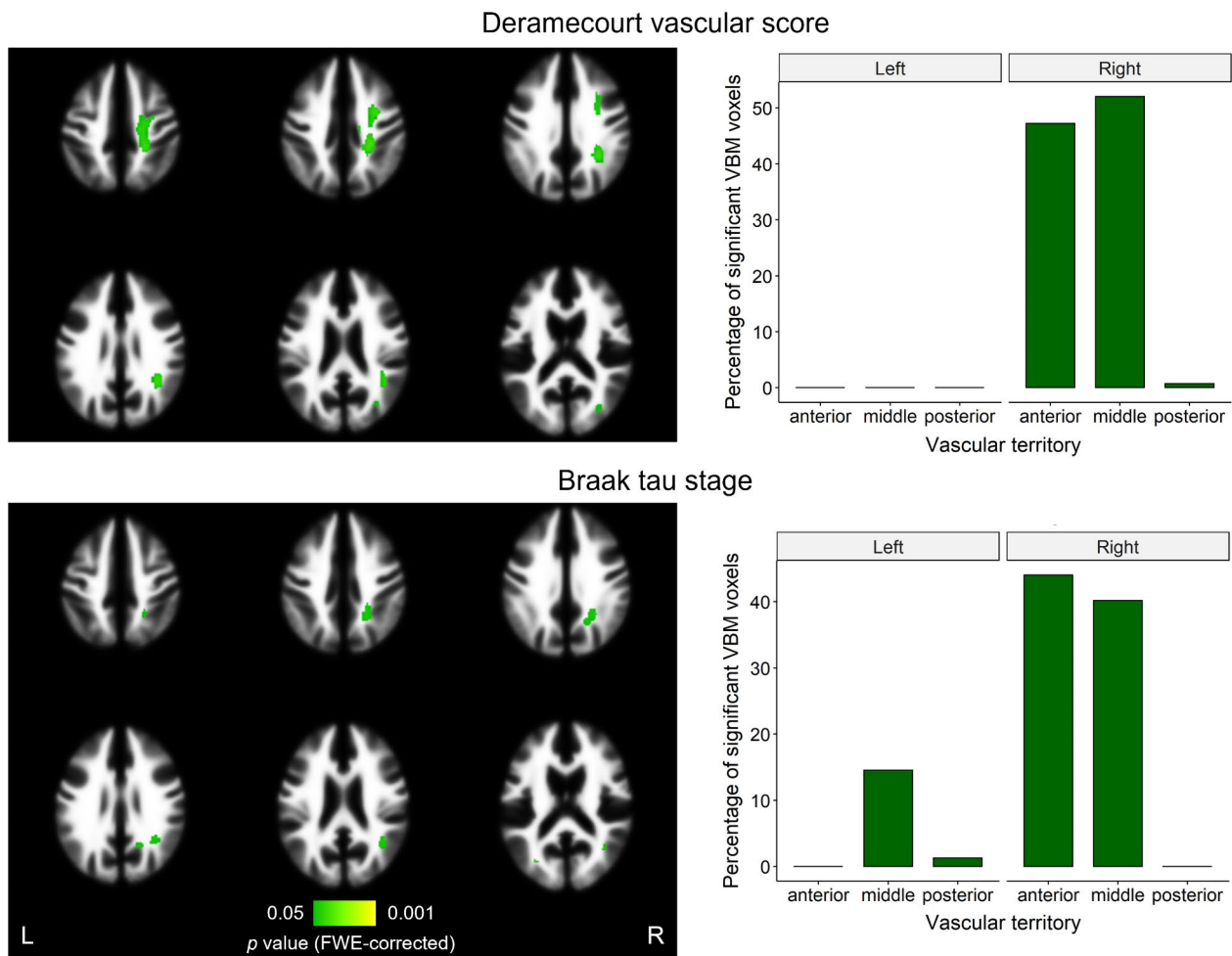


Fig. 5 VBM results on WMH maps as a function of neuropathologies. After applying threshold-free cluster enhancement and FWE correction on the WM region, significant results ($p < 0.05$) were found as a function of Deramecourt vascular score and tau stage. On the left, significant effects (in green) are overlaid on the WM tissue probability map from SPM12, with left and right sides indicated. Colormap indicates FWE-corrected p values. On the right, the percentage of each of these significant effects falling into each region of the vascular territory atlas (regions perfused by anterior, middle, and posterior cerebral arteries) is shown. FWE=family-wise error; L=left; R=right; VBM=voxel-based morphometry; WMH=white matter hyperintensity

correlated with WMH burden in the right hemisphere. Considering WMH burden did not quantitatively differ between hemispheres, and that our neuropathological evaluation was based on the left one, these results might reflect a more compact topography of right-hemisphere lesions, favoring their correlation through VBM, rather than a lateralization of pathology effects.

The histopathological assessment of vascular pathology in dementia is highly variable [28]. We report a robust association of the Deramecourt vascular staging [35] with WMH burden, which in turn is known to relate to specific vascular lesions such as CAA [21], microinfarcts and arteriolosclerosis [25]. Although this staging system assumes a sequential order between vascular events, we further report its ability to capture the relationship between WMHs and vessel wall modifications, supporting its value as a clinically relevant descriptor of vascular

pathology. In contrast, while the VCING consensus evaluation [36] was also linked to higher WMH volumes, it exhibited no significant contribution in the combined pathology model. Similarly, no effects were found for CAA severity evaluated by VCING criteria, despite the previously reported link between CAA and WMHs [44], potentially exacerbated by AD pathology [45]. These findings could inform the prioritization between Deramecourt and VCING staging systems in future studies. Furthermore, they underscore the need for refined criteria that unify the strengths of both systems to better capture the contribution of vascular pathology to dementia and its associated MRI phenotypes.

Our results also highlight the structural impact of hippocampal sclerosis of aging. Although the contribution of HS to a worsened cognitive state is well documented [46, 47], this pathology is often overlooked in voxel-wise

MRI studies [7, 9]. Other authors exploring volumetric differences have reported an independent impact of HS on atrophy of the hippocampus [10, 48] and neighboring GM [11]. A recent study also found that while the clinical presence of dementia independently impacts hippocampal atrophy and overcomes the effects of most pathologies, it does not surpass those of HS [49]. In the current cohort, of advanced age and primarily female, the effects of HS on grey matter atrophy were found to overshadow those of any other coexisting pathology. These findings may point towards our recently proposed HS staging [37] as a more accurate descriptor of neurodegeneration compared to LATE stage, as despite their correlation, only the former displayed significant effects in the combined model. We also found a significant effect of HS on WMH burden in a subset of the cohort with shorter antemortem interval, and thereby a reduced time span between both measurements. This result could reflect an independent relation between HS-associated grey matter atrophy and WMHs, which has been previously explored in the context of global brain atrophy [50]. Interestingly, we did not find hippocampal GMD among the regions with strongest correlation to cognitive performance, which may reflect neurodegenerative progression such that regions outside the medial temporal lobe become critical in sustaining cognitive function at advanced disease stages.

In this study, neuropathologies were assessed following consensus criteria, and thereby assumed to present homogeneous spatial distributions across patients. This represents a potential limitation compared to studies specifically measuring regional pathology burdens in relation to *in vivo* alterations [8, 51]. Similarly, vascular pathology events were not independently assessed, limiting the evaluation of more detailed, regional associations. Additionally, the sample size was defined by the availability of patient MRI and brain donation and not specifically designed for these combined analyses, which results in modest effect sizes, especially in quantitative WMH results. Another limitation of this work is the joint measurement of periventricular and deep WMHs, as some authors have suggested these present differing clinical phenotypes and microstructural changes [52]. On the other hand, the comparison of several automated, data-agnostic WMH quantification method is a strength of this study. The selected Lesion Prediction Algorithm (LPA) was especially robust in segmenting deep lesions, and has been previously demonstrated to provide accurate results with respect to manual labelling [53]. Other strengths of this work include the use of “lesion filling” strategies to optimize GM/WM delineation in the presence of WMHs, and the implementation of time corrections to partially overcome a long mean AMI resulting from scanning difficulties in dementia patients.

Conclusion

Taken together, this study provides evidence that in dementia patients with an amnesic profile, grey matter atrophy is primarily driven by HS and ADNC, while WMH burden is most strongly associated with cerebrovascular and tau pathologies. Our analyses also inform the spatial signatures of these associations and the performance of different methodologies within the heterogeneous landscape of WMH and vascular pathology assessment. Furthermore, this work highlights the relevance of comprehensive pathological evaluations in post-mortem studies and has implications for the use of structural MRI within diagnostic protocols. More specifically, our findings reinforce doubts about the suitability of WMHs as a biomarker of vascular dementia [54]. In this context, the assessment of WMHs as an intermediary marker of brain damage, rather than a diagnostic criterium, has been proposed [17]. The combination of this measure with other techniques such as arterial spin labeling (ASL) or diffusion MRI, both with recent methodological advances applied to the study of cognitive decline [55–57], could be valuable towards a more specific *in vivo* identification of vascular alterations.

Abbreviations

AAL3	Automated Anatomical Labelling Atlas 3
AD	Alzheimer's Disease
ADNC	Alzheimer's Disease Neuropathological Change
AMI	Antemortem interval
ASL	Arterial spin labeling
A β	Amyloid- β
BT-CIEN	CIEN Foundation brain bank ('Banco de Tejidos Fundación CIEN', in Spanish)
CAA	Cerebral amyloid angiopathy
CAT12	Computational Anatomy Toolbox
DARTEL	Diffeomorphic Atlas Registration Tool with Exponentiated Lie Algebras
DLB	Dementia with Lewy Bodies
FLAIR	Fluid-attenuated inversion recovery
FSE	Fast spin echo
FSPGR	Fast spoiled gradient recalled
FTD	Frontotemporal Dementia
FWE	Family-wise error
GLM	Generalized linear model
GM	Grey matter
GMD	Grey matter density
H/E	Hematoxylin/eosin
HS	Hippocampal sclerosis of aging
LATE	Limbic-predominant age-related TDP-43 encephalopathy
LB	Lewy body
LGA	Lesion Growth Algorithm
LPA	Lesion Prediction Algorithm
LST	Lesion Segmentation Toolbox
MNI	Montreal Neurological Institute
MRI	Magnetic resonance imaging
sMMSE	Severe Mini-Mental State Examination
TIV	Total intracranial volume
VACS	Vallecas Alzheimer's Center Study
VaD	Vascular dementia
VBM	Voxel-based morphometry
VCING	Vascular Cognitive Impairment Neuropathology Guidelines
WMH	White matter hyperintensity

Supplementary Information

The online version contains supplementary material available at <https://doi.org/10.1186/s13195-024-01633-2>.

Supplementary Material 1

Acknowledgements

We wish to thank the participants of the VACS cohort and their family members, as well as the Queen Sofia Foundation and CIEN Foundation staff who made possible the collection of this dataset. Especially, we would like to thank Eva Alfayate, Felipe García and Linda Zhang from the neuroimaging department.

Author contributions

BAS supervised study design, analyses and interpretation. AR performed all neuropathological evaluations and aided with result interpretation. DOC analyzed, interpreted the data, and was a major contributor in writing the manuscript. All authors reviewed and approved the final manuscript.

Funding

The collection of data for this work has been supported by the Queen Sofia Foundation and the CIEN Foundation. DOC was supported by "la Caixa" Foundation (ID 100010434), with fellowship code LCF/BQ/DR20/11790034. BAS was supported by an MIT International Science and Technology Initiative Global Seed Fund (0000000246).

Data availability

The data analyzed for the current study are available from the CIEN Foundation but restrictions apply to their availability due to personal data protections reasons. Anonymized data are however available from the corresponding author upon reasonable request.

Declarations

Ethics approval and consent to participate

The BT-CIEN brain bank is an officially registered biobank by the Carlos III Research Institute (Ref: 741). BT-CIEN procedures, as well as VACS cohort patient follow-up have been approved by local health authorities (Ref: MCB/RMSFC, Expte: 12672). All brain donations were carried out under informed consent by a relative or proxy, as approved by the Ethics Committee of the Carlos III Research Institute. The study of these data was independently approved by the ethics committee of the Universidad Politécnica de Madrid (No Expte: 2021-062).

Consent for publication

The Vallecas Alzheimer's Center Study was designed between 2005 and 2006 by the CIEN Foundation with consultation of the Ethics Committee and local health authorities. Following national regulations at the time, and due to the sensitivity of the data collected, consent for publication was not included in the informed consent forms used for this study.

Competing interests

The authors declare no competing interests.

Received: 1 September 2024 / Accepted: 29 November 2024

Published online: 09 January 2025

References

- Knopman DS, DeKosky ST, Cummings JL, et al. Practice parameter: diagnosis of dementia (an evidence-based review). *Neurology*. 2001;56(9):1143–53. <https://doi.org/10.1212/WNL.56.9.1143>.
- Brien O JT. Role of imaging techniques in the diagnosis of dementia. *Br J Radiol*. 2007;80(Spec N 2):S71–7. <https://doi.org/10.1259/bjr/33117326>.
- Sorbi S, Hort J, Erkinjuntti T, et al. EFNS-ENS guidelines on the diagnosis and management of disorders associated with dementia. *Eur J Neurol*. 2012;19(9):1159–79. <https://doi.org/10.1111/j.1468-1331.2012.03784.x>.
- Koikkalainen J, Rhodius-Meester H, Tolonen A, et al. Differential diagnosis of neurodegenerative diseases using structural MRI data. *NeuroImage Clin*. 2016;11:435–49. <https://doi.org/10.1016/j.nicl.2016.02.019>.
- Schneider JA, Arvanitakis Z, Bang W, et al. Mixed brain pathologies account for most dementia cases in community-dwelling older persons. *Neurology*. 2007;69(24):2197–204. <https://doi.org/10.1212/01.wnl.0000271090.28148.24>.
- Hanko V, Apple AC, Alpert KI, et al. In-Vivo hippocampal subfield shape related to TDP-43, amyloid beta, and tau pathologies. *Neurobiol Aging*. 2019;74:171. <https://doi.org/10.1016/j.neurobiolaging.2018.10.013>.
- Bejanin A, Murray ME, Martin P, et al. Antemortem volume loss mirrors TDP-43 staging in older adults with non-frontotemporal lobar degeneration. *Brain*. 2019;142(11):3621–35. <https://doi.org/10.1093/brain/awz277>.
- de Flores R, Wisse LEM, Das SR, et al. Contribution of mixed pathology to medial temporal lobe atrophy in Alzheimer's disease. *Alzheimers Dement*. 2020;16(6):843–52. <https://doi.org/10.1002/ALZ.12079>.
- Teipel SJ, Fritz HC, Grothe MJ. Neuropathologic features associated with basal forebrain atrophy in Alzheimer disease. *Neurology*. 2020;95(10):E1301–11. <https://doi.org/10.1212/WNL.00000000000010192>.
- Dawe RJ, Bennett DA, Schneider JA, et al. Neuropathologic correlates of hippocampal atrophy in the Elderly: a clinical, pathologic, postmortem MRI study. *PLoS ONE*. 2011;6(10):e26286. <https://doi.org/10.1371/JOURNAL.PONE.0026286>.
- Kotrotsou A, Schneider JA, Bennett DA, et al. Neuropathologic correlates of regional brain volumes in a community cohort of older adults. *Neurobiol Aging*. 2015;36(10):2798–805. <https://doi.org/10.1016/j.neurobiolaging.2015.06.025>.
- Román GC, Tatemichi TK, Erkinjuntti T et al. Vascular dementia: Diagnostic criteria for research studies. Report of the NINDS-AIREN International Workshop. *Neurology*. 1993;43:250–60. <https://doi.org/10.1212/wnl.43.2.250>.
- Hachinski V, Iadecola C, Petersen RC, et al. National Institute of Neurological Disorders and stroke–Canadian Stroke Network Vascular Cognitive Impairment Harmonization standards. *Stroke*. 2006;37(9):2220–41. <https://doi.org/10.1161/01.STR.0000237236.88823.47>.
- Sachdev P, Kalaria R, O'Brien J, et al. Diagnostic criteria for vascular cognitive disorders: a VASCOG statement. *Alzheimer Dis Assoc Disord*. 2014;28(3):206–18. <https://doi.org/10.1097/WAD.0000000000000034>.
- Prins ND, Scheltens P. White matter hyperintensities, cognitive impairment and dementia: an update. *Nat Rev Neurol*. 2015;11(3):157–65. <https://doi.org/10.1038/NRNEUROL.2015.10>.
- DeBette S, Markus HS. The clinical importance of white matter hyperintensities on brain magnetic resonance imaging: systematic review and meta-analysis. *BMJ*. 2010;341(7767):288. <https://doi.org/10.1136/BMJ.C3666>.
- Wardlaw JM, Valdés Hernández MC, Muñoz-Maniega S. What are white matter hyperintensities made of? Relevance to vascular cognitive impairment. *J Am Heart Assoc*. 2015;4(6):001140. <https://doi.org/10.1161/JAHA.114.001140>.
- Hase Y, Horsburgh K, Ihara M, et al. White matter degeneration in vascular and other ageing-related dementias. *J Neurochem*. 2018;144(5):617–33. <https://doi.org/10.1111/jnc.14271>.
- Fazekas F, Chawluk JB, Alavi A. MR signal abnormalities at 1.5 T in Alzheimer's dementia and normal aging. *Am J Neuroradiol*. 1987;8(3):421–6. <https://doi.org/10.2214/ajr.149.2.351>.
- Scheltens P, Barkhof F, Leys D, et al. A semiquantitative rating scale for the assessment of signal hyperintensities on magnetic resonance imaging. *J Neurol Sci*. 1993;114(1):7–12. [https://doi.org/10.1016/0022-510X\(93\)90041-V](https://doi.org/10.1016/0022-510X(93)90041-V).
- Alosco ML, Sugarman MA, Besser LM, et al. A Clinicopathological Investigation of White Matter hyperintensities and Alzheimer's Disease Neuropathology. *J Alzheimers Dis*. 2018;63(4):1347–60. <https://doi.org/10.3233/JAD-180017>.
- Lee H, Wiggermann V, Rauscher A, et al. Brain imaging abnormalities in mixed Alzheimer's and subcortical vascular dementia. *Can J Neurol Sci*. 2022;1–14. <https://doi.org/10.1017/cjn.2022.65>.
- Wei K, Tran T, Chu K, et al. White matter hypointensities and hyperintensities have equivalent correlations with age and CSF β -amyloid in the nondemented elderly. *Brain Behav*. 2019;9(12):1–9. <https://doi.org/10.1002/brb3.11457>.
- Graff-Radford J, Arenaza-Urquijo EM, Knopman DS, et al. White matter hyperintensities: relationship to amyloid and tau burden. *Brain*. 2019;142(8):2483–91. <https://doi.org/10.1093/brain/awz162>.
- Arfanakis K, Evia AM, Leurgans SE, et al. Neuropathologic Correlates of White Matter Hyperintensities in a community-based cohort of older adults. *J Alzheimers Dis*. 2020;73(1):333–45. <https://doi.org/10.3233/JAD-190687>.

26. McAleese KE, Firbank M, Dey M, et al. Cortical tau load is associated with white matter hyperintensities. *Acta Neuropathol Commun.* 2015;3:60. <https://doi.org/10.1186/s40478-015-0240-0>.
27. Kapasi A, Yu L, Petyuk V, et al. Association of small vessel disease with tau pathology. *Acta Neuropathol.* 2022;143(3):349–62. <https://doi.org/10.1007/s00401-021-02397-x>.
28. Kovacs GG, Alafuzoff I, Al-Sarraj S, et al. Mixed brain pathologies in dementia: the BrainNet Europe consortium experience. *Dement Geriatr Cogn Disord.* 2008;26(4):343–50. <https://doi.org/10.1159/000161560>.
29. McAleese KE, Colloby SJ, Thomas AJ, et al. Concomitant neurodegenerative pathologies contribute to the transition from mild cognitive impairment to dementia. *Alzheimer's Dement.* 2021;17(7):1121–33. <https://doi.org/10.1002/alz.12291>.
30. Harrell LE, Marson D, Chatterjee A, et al. The severe Mini-mental State examination: a new neuropsychologic instrument for the bedside assessment of severely impaired patients with Alzheimer disease. *Alzheimer Dis Assoc Disord.* 2000;14(3):168–75. <https://doi.org/10.1097/00002093-200007000-00008>.
31. Martínez-Martín P, Ávila J, Investigators ARU. Alzheimer Center Reina Sofia Foundation: fighting the Disease and providing overall solutions. *J Alzheimer's Dis.* 2010;21(2):337–48. <https://doi.org/10.3233/JAD-2010-101149>.
32. Montine TJ, Phelps CH, Beach TG, et al. National institute on aging-Alzheimer's association guidelines for the neuropathologic assessment of Alzheimer's disease: a practical approach. *Acta Neuropathol.* 2012;123(1):1–11. <https://doi.org/10.1007/s00401-011-0910-3>.
33. Braak T, Rüb, et al. Staging of brain pathology related to sporadic Parkinson's disease. *Neurobiology of Aging.* Elsevier BV; 2003;24:197. [https://doi.org/10.1016/s0197-4580\(02\)00065-9](https://doi.org/10.1016/s0197-4580(02)00065-9).
34. Nelson PT, Dickson DW, Trojanowski JQ, et al. Limbic-predominant age-related TDP-43 encephalopathy (LATE): consensus working group report. *Brain.* 2019;142(6):1503–27. <https://doi.org/10.1093/brain/awz099>.
35. Deramecourt V, Slade J, Oakley A, et al. Staging and natural history of cerebrovascular pathology in dementia. *Neurology.* 2012;78(14):1043–50. <https://doi.org/10.1212/WNL.0b013e31824e8e7f>.
36. Skrobot OA, Attems J, Esiri M, et al. Vascular cognitive impairment neuropathology guidelines (VCING): the contribution of cerebrovascular pathology to cognitive impairment. *Brain.* 2016;139(11):2957–69. <https://doi.org/10.1093/Brain/AWW214>.
37. Ortega-cruz D, Uceda-heras A, Strange B, et al. A novel histological staging of hippocampal sclerosis that is evident in gray matter loss in vivo. *Alzheimer's Dement.* 2023;19(7):3028–40. <https://doi.org/10.1002/alz.12942>.
38. Gaser C, Dahnke R, Thompson P, et al. CAT – a computational anatomy toolbox for the analysis of Structural MRI Data. *bioRxiv.* 2022. <https://doi.org/10.1101/2022.06.11.495736>.
39. Schmidt P, Wink L. LST: A lesion segmentation tool for SPM. 2019. pp. 6–9. <https://www.statistical-modelling.de/lst.html>
40. Cerri S, Puonti O, Meier DS, et al. A contrast-adaptive method for simultaneous whole-brain and lesion segmentation in multiple sclerosis. *NeuroImage.* 2021;225:117471. <https://doi.org/10.1016/j.neuroimage.2020.117471>.
41. Smith SM, Nichols TE. Threshold-free cluster enhancement: addressing problems of smoothing, threshold dependence and localisation in cluster inference. *NeuroImage.* 2009;44(1):83–98. <https://doi.org/10.1016/J.NEUROIMAGE.2008.03.061>.
42. Rolls ET, Huang CC, Lin CP et al. Automated anatomical labelling atlas 3. *Neuroimage.* 2020;206(August 2019):116189. <https://doi.org/10.1016/j.neuroimage.2019.116189>
43. Schirmer MD, Giese AK, Fotiadis P, et al. Spatial signature of White Matter hyperintensities in Stroke patients. *Front Neurol.* 2019;10(208):1–10. <https://doi.org/10.3389/fneur.2019.00208>.
44. Shirzadi Z, Yau WYW, Schultz SA, et al. Progressive White Matter Injury in pre-clinical Dutch cerebral amyloid Angiopathy. *Ann Neurol.* 2022;92(3):358–63. <https://doi.org/10.1002/ANA.26429>.
45. Lee S, Zimmerman ME, Narkhede A, et al. White matter hyperintensities and the mediating role of cerebral amyloid angiopathy in dominantly-inherited Alzheimer's disease. *PLoS ONE.* 2018;13(5):e0195838. <https://doi.org/10.1371/JOURNAL.PONE.0195838>.
46. Dickson DW, Davies P, Bevona C, et al. Hippocampal sclerosis: a common pathological feature of dementia in very old (≥ 80 years of age) humans. *Acta Neuropathol.* 1994;88(3):212–21. <https://doi.org/10.1007/BF00293396>.
47. Nelson PT, Smith CD, Abner EL, et al. Hippocampal sclerosis of aging, a prevalent and high-morbidity brain disease. *Acta Neuropathol.* 2013;126(2):161–77. <https://doi.org/10.1007/s00401-013-1154-1>.
48. Woodworth DC, Nguyen HL, Khan Z, et al. Utility of MRI in the identification of hippocampal sclerosis of aging. *Alzheimer's Dement.* 2021;17(5):847–55. <https://doi.org/10.1002/alz.12241>.
49. Woodworth DC, Sheikh-Bahaei N, Scambray KA, et al. Dementia is associated with medial temporal atrophy even after accounting for neuropathologies. *Brain Commun.* 2022;4(2). <https://doi.org/10.1093/BrainComms/FCAC052>.
50. Appelman APA, Exalto LG, Van Der Graaf Y, et al. White matter lesions and brain atrophy: more than shared risk factors? A systematic review. *Cerebrovasc Dis.* 2009;28(3):227–42. <https://doi.org/10.1159/000226774>.
51. Blanken AE, Hurtz S, Zarow C, et al. Associations between hippocampal morphology and neuropathologic markers of Alzheimer's disease using 7 T MRI. *NeuroImage Clin.* 2017;15:56–61. <https://doi.org/10.1016/j.nicl.2017.04.020>.
52. Griffanti L, Jenkinson M, Suri S, et al. Classification and characterization of periventricular and deep white matter hyperintensities on MRI: a study in older adults. *NeuroImage.* 2018;170:174–81. <https://doi.org/10.1016/j.neuroimage.2017.03.024>.
53. Ribaldi F, Altomare D, Jovicich J, et al. Accuracy and reproducibility of automated white matter hyperintensities segmentation with lesion segmentation tool: a European multi-site 3T study. *Magn Reson Imaging.* 2021;76:108–15. <https://doi.org/10.1016/j.mri.2020.11.008>.
54. Shirzadi Z, Schultz SA, Yau WYW, et al. Etiology of White Matter hyperintensities in autosomal Dominant and sporadic Alzheimer Disease. *JAMA Neurol.* 2023;80(12):1353–63. <https://doi.org/10.1001/jamaneurol.2023.3618>.
55. Huang D, Guo Y, Guan X, et al. Recent advances in arterial spin labeling perfusion MRI in patients with vascular cognitive impairment. *J Cereb Blood Flow Metab.* 2023;43(2):173–84. <https://doi.org/10.1177/0271678X221135353>.
56. Raghavan S, Przybelski SA, Reid RI, et al. White matter damage due to vascular, tau, and TDP-43 pathologies and its relevance to cognition. *Acta Neuropathol Commun.* 2022;10(1):1–14. <https://doi.org/10.1186/s40478-022-01319-6>.
57. Dewenter A, Jacob MA, Cai M, et al. Disentangling the effects of Alzheimer's and small vessel disease on white matter fibre tracts. *Brain.* 2023;146(2):678–89. <https://doi.org/10.1093/brain/awac265>.

Publisher's note

Springer Nature remains neutral with regard to jurisdictional claims in published maps and institutional affiliations.